Computers & Fluids 38 (2009) 883–887

Contents lists available at ScienceDirect

Computers & Fluids

journal homepage: www.elsevier.com/locate/compfluid

A unified approach for nonslip and slip boundary conditions in the lattice Boltzmann method

Long-Sheng Kuo, Ping-Hei Chen *

Department of Mechanical Engineering, National Taiwan University, No. 1, Sec. 4, Roosevelt Road, Taipei 10617, Taiwan

ARTICLE INFO

Article history:
Received 10 January 2008
Received in revised form 20 June 2008
Accepted 23 September 2008
Available online 4 October 2008

ABSTRACT

This work proposed a unified approach to impose both nonslip and slip boundary conditions for the lattice Boltzmann method (LBM). By introducing the tangential momentum accommodation coefficient (TMAC), the present implementation can determine the change of the tangential momentum on the wall and then impose the correct boundary conditions for LBM. The simulation results demonstrate that this implementation is equivalent to the first-order slip model.

1. Introduction

The lattice Boltzmann method (LBM) has been proved a powerful numerical tool for fluid mechanics since it can recover the Navier–Stokes equations with Chapman–Enskog expansions. In the beginning of the development, a lot of researches focused on the problems in which nonslip boundary conditions were applicable. The most popular scheme applied is the bounce-back scheme because of its easy implementation. However, the bounce-back scheme has been proved that it would generate a nonzero slip velocity [1]. There were then several works to impose correct nonslip boundary conditions in LBM [2–8].

On the other hand, the developments of micro-electro-mechanical systems (MEMS) and nano-technology have stimulated the study of the systems with micro-scale sizes, such as microchannel flows. In such the scale range, the mean free path of the fluid could be the same order as the geometric size of the devices. Thus, the Knudsen layer is large and the nonslip boundary conditions are no longer valid. Therefore, many researches have applied the LBM with various slip boundary conditions to the microscale fluid systems [9–17]. Since the specular reflection implies slippage, a popular slip boundary scheme introduced two parameters (r and s, $r+s=1$) to adjust the weighting of distributions on the wall between bounce-back and specular reflections [10,11,16,17]. When $r=1$, it recovers the bounce-back scheme. Their physical boundaries locates between nodes and their slip velocity is the velocity at the nodes nearest to the wall, not the velocity on the wall. To get the ordinary slip velocity, an extrapolation is required [11]. Therefore, if a fair comparison between the numerical work and the theoretical analysis is desired, either an extrapolation of the numerical work or an interpolation of the theoretical work should be made.

The purpose of this work is then to propose a unified approach for non-slip and slip boundary conditions in LBM. First, the microscopic point of view of the slip phenomena is reviewed. The key point is the tangential momentum change caused by the boundary. With the help of the tangential momentum accommodation coefficient (TMAC, σ) [18], one can know the change of the tangential momentum of the fluid on the wall. Therefore, correct boundary conditions can be imposed for LBM. In addition, the present scheme locate the nodes on the physical boundaries. This makes the verifications of boundary conditions more directly, no extrapolations or interpolations required. The present scheme is applicable to either nonslip or slip boundary conditions. The numerical results show that this scheme is equivalent to the first-order slip model [18].

2. Slip phenomena and tangential momentum accommodation coefficient

From the microscopic point of view, when the fluidic particles are specularly reflected, the tangential velocity are preserved. It implies that the wall would not exert tangential stresses on the fluid (shear stress free) and slippage would be observed. On the other hand, if the wall exerts tangential stresses on the fluid, the tangential momentum would be altered after reflection. To determine the momentum change, one can first calculate the incident tangential momentum (P_I) by

$$P_I \equiv \int_{\mathbf{v}\cdot\mathbf{n}\leqslant 0} (f\mathbf{v})_{\parallel} d\mathbf{v} \tag{1}$$

where f is the mass density distribution of the fluid, $\mathbf{n}$ is the normal direction of the wall toward the fluid field, and $\mathbf{v}_{\parallel}$ is the velocity in the tangential direction. From the macroscopic point of view, P_I can be expressed by the product of the density and the velocity:

* Corresponding author. Tel./fax: +886 2 23670781.
E-mail address: phchen@ntu.edu.tw (P.-H. Chen).

0045-7930/$ - see front matter © 2008 Elsevier Ltd. All rights reserved.
doi:10.1016/j.compfluid.2008.09.008

$$\rho_I \equiv \int_{\mathbf{v}\cdot\mathbf{n}\leqslant 0} f d\mathbf{v}, \quad P_I \equiv \rho_I U_I \tag{2}$$

where ρ_I is the density of the incident particles on the boundary, and U_I is the incident tangential velocity. Similarly, the reflected parts are

$$\rho_R \equiv \int_{\mathbf{v}\cdot\mathbf{n}\geqslant 0} f d\mathbf{v}, \quad P_R \equiv \int_{\mathbf{v}\cdot\mathbf{n}\geqslant 0} (f\mathbf{v})_{\parallel} d\mathbf{v} = \rho_R U_R. \tag{3}$$

Meanwhile, the overall average density, ρ, and the overall average tangential velocity of the fluid on the boundary, U, are determined by

$$\rho \equiv \int f d\mathbf{v} = \left(\int_{\mathbf{v}\cdot\mathbf{n}\leqslant 0} + \int_{\mathbf{v}\cdot\mathbf{n}\geqslant 0}\right) f d\mathbf{v} = \rho_I + \rho_R \tag{4}$$

$$\rho U \equiv \int (f\mathbf{v})_{\parallel} d\mathbf{v} = \int_{\mathbf{v}\cdot\mathbf{n}\leqslant 0} (f\mathbf{v})_{\parallel} d\mathbf{v} + \int_{\mathbf{v}\cdot\mathbf{n}\geqslant 0} (f\mathbf{v})_{\parallel} d\mathbf{v} = \rho_I U_I + \rho_R U_R. \tag{5}$$

From the mass conservation and to avoid particle accumulations on the boundaries, the reflected fluid should be equal to the incident fluid for an impermeable boundary. Therefore, $\rho_I = \rho_R = \rho/2$.

To describe the effect of the boundary on the tangential momentum of the fluid, the tangential momentum accommodation coefficient σ (TMAC) is defined as [18,19]

$$\sigma \equiv \frac{\rho_R U_R - \rho_I U_I}{\rho_R U_W - \rho_I U_I} = \frac{U_R - U_I}{U_W - U_I} \tag{6}$$

where U_W is the tangential velocity of the wall. Thus, the velocity U can be expressed by

$$U = \frac{1}{\rho}(\rho_I U_I + \rho_R U_R) = \frac{1}{2}\sigma U_W + \left(1 - \frac{\sigma}{2}\right) U_I. \tag{7}$$

When $\sigma = 0$, it means no shear stress acts on the fluid and the wall is a slip boundary. On the other hand, if σ=2, $U = U_W$ and it is the non-slip boundary condition.

In order to consider the effect of the permeation, and to describe the effects of the boundary on the tangential momentums with the macroscopic quantities, e.g., ρ and U, a modified tangential momentum accommodation coefficient, σ', is defined by

$$\sigma' \equiv \frac{U - U_{SR}}{U_W - U_{SR}} \tag{8}$$

where U_{SR} is the average tangential velocity under the specular reflection by the impermeable boundary, which is equal to U_I. The relation between σ and σ' is

$$\sigma' = \frac{\rho U - \rho U_{SR}}{\rho U_W - \rho U_{SR}} = \frac{(\rho_I U_I + \rho_R U_R) - (\rho_I + \rho_R) U_I}{\rho(U_W - U_I)} = \frac{\rho_R}{\rho}\frac{U_R - U_I}{U_W - U_I} = \frac{\rho_R}{\rho}\sigma. \tag{9}$$

For an impermeable boundary, $\sigma = 2\sigma'$. The tangential momentum change of the fluid caused by the boundary can be also determined by

$$\rho(U - U_{SR}) = \sigma'\rho(U_W - U_{SR}). \tag{10}$$

If U_{SR} can be expressed by the Taylor expansion at the wall about one mean free path (λ) away,

$$U_{SR} \approx U + \lambda \left.\frac{\partial U}{\partial n}\right|_w + \cdots, \tag{11}$$

then the slip velocity, $U - U_W$, can be calculated by

$$U - U_W \approx \frac{1 - \sigma'}{\sigma'} \lambda \left.\frac{\partial U}{\partial n}\right|_w. \tag{12}$$

This is the first-order slip model [18].

3. General description of LBM

The lattice Boltzmann equation with BGK relaxation time approximation can be written as.

$$f_i(\mathbf{x} + \mathbf{c}_i\Delta t, t + \Delta t) - f_i(\mathbf{x}, t) = \frac{\Delta t}{\tau}\left[f_i^{eq}(\mathbf{x}, t) - f_i(\mathbf{x}, t)\right] \tag{13}$$

where $\mathbf{c}_i$ is the basis vector of the lattice, τ is the relaxation time constant for the flow field, and the superscript eq denotes the distribution at equilibrium. The density, ρ, velocity, $\mathbf{u}$, of the fluid are determined by

$$\rho = \sum_i f_i, \qquad \rho\mathbf{u} = \sum_i f_i \mathbf{c}_i. \tag{14}$$

In this study, the D2Q9 lattice is used as illustration. For D2Q9 lattice, the nine basis vectors are given by

$$\mathbf{c}_i = \begin{cases} \mathbf{0}, & i = 0 \\ \cos\left(\frac{(i-1)\pi}{2}\right)\mathbf{i}_x + \sin\left(\frac{(i-1)\pi}{2}\right)\mathbf{i}_y, & i = 1 \sim 4 \\ \sqrt{2}\left[\cos\left(\frac{(2i-1)\pi}{4}\right)\mathbf{i}_x + \sin\left(\frac{(2i-1)\pi}{4}\right)\mathbf{i}_y\right], & i = 5 \sim 8 \end{cases} \tag{15}$$

The corresponding equilibrium distributions are

$$f_i^{eq} = \rho w_i\left[1 + 3\mathbf{u}\cdot\mathbf{c}_i + \frac{9}{2}(\mathbf{u}\cdot\mathbf{c}_i)^2 - \frac{3}{2}|\mathbf{u}|^2\right] \tag{16}$$

where $w_0 = 4/9$, $w_1 = w_2 = w_3 = w_4 = 1/9$, $w_5 = w_6 = w_7 = w_8 = 1/36$. The macroscopic transport property of the fluid like kinematic viscosity v is determined by

$$v = \frac{1}{3}\left(\frac{\tau}{\Delta t} - \frac{1}{2}\right). \tag{17}$$

4. Slip boundary conditions in LBM

For a boundary with given σ' and the permeation velocity U_P, the unknown distributions of the boundary nodes are contributed from three parts: the specular reflection (f_i^{sr}), the stress exerted by the wall (f_i^w), and the permeation condition (f_i^p):

$$f_i = f_i^{sr} + f_i^w + f_i^p \tag{18}$$

where the subscript i of the unknown distributions satisfies $\mathbf{c}_i \cdot \mathbf{n} > 0$. Each part can be treated individually as follows. First, the specular-reflection is readily determined if the boundary is horizontal or vertical. For example, the unknown distributions for a upper horizontal wall are f_4, f_7 and f_8. Thus, $f_4^{sr} = f_2$, $f_7^{sr} = f_6$, $f_8^{sr} = f_5$.

Once f_i^{sr} are determined, U_{SR} can be calculated by

$$\rho = \sum_i f_i \tag{19}$$

$$\rho U_{SR} = \sum_{\mathbf{c}_i\cdot\mathbf{n}\leqslant 0} (f_i\mathbf{c}_i)_{\parallel} + \sum_{\mathbf{c}_i\cdot\mathbf{n}>0} (f_i^{sr}\mathbf{c}_i)_{\parallel}. \tag{20}$$

The change of the tangential momentum caused by the wall is contributed by unknown f_i^w.

$$\sigma'\rho(U_W - U_{SR}) = \sum_{\mathbf{c}_i\cdot\mathbf{n}>0} (f_i^w\mathbf{c}_i)_{\parallel} \tag{21}$$

$$0 = \sum_{\mathbf{c}_i\cdot\mathbf{n}>0} (f_i^w\mathbf{c}_i)_{\perp} \tag{22}$$

$$0 = f_i^w \quad \text{for normal direction.} \tag{23}$$

The zero sum of the normal parts in Eq. (22) makes sure that f_i^w's alter the tangential momentum only. It also implies $\sum f_i^w$ will not contribute to the density calculation.

If the boundary is permeable, the permeation conditions are counted by

$$\rho U_P = \sum_{\mathbf{c}_i\cdot\mathbf{n}\leqslant 0} (f_i\mathbf{c}_i)_\perp + \sum_{\mathbf{c}_i\cdot\mathbf{n}>0} (f_i^p\mathbf{c}_i)_\perp \tag{24}$$

$$0 = \sum_{\mathbf{c}_i\cdot\mathbf{n}>0} (f_i^p\mathbf{c}_i)_\parallel. \tag{25}$$

The zero sum of the tangential velocity of f_i^p in Eq. (25) guarantees that f_i^p won't affect the calculation of the tangential momentum.

4.1. D2Q9 lattice

Consider a lower flat boundary in D2Q9 lattice as an example. The tangential direction is in x direction, and the normal direction is in $+y$ direction. The unknown distributions after streaming processes are f_2, f_5, and f_6. The corresponding specular-reflection distributions are then

$$f_2^{sr} = f_4, \qquad f_5^{sr} = f_8, \qquad f_6^{sr} = f_7 \tag{26}$$

$$\rho U_{SR} = f_1 - f_3 + 2(f_8 - f_7). \tag{27}$$

The shear stress exerted by the wall leads to the momentum change.

$$\sigma'\rho(U_W - U_{SR}) = \sum_{\mathbf{c}_i\cdot\mathbf{n}>0} (f_i^w\mathbf{c}_i)_x = f_5^w - f_6^w \tag{28}$$

$$0 = \sum_{\mathbf{c}_i\cdot\mathbf{n}>0} (f_i^w\mathbf{c}_i)_y = f_2^w + f_5^w + f_6^w = f_5^w + f_6^w \tag{29}$$

where $f_2^w = 0$. Therefore,

$$f_5^w = \frac{\sigma'\rho}{2}(U_W - U_{SR}), \quad f_6^w = -f_5^w. \tag{30}$$

If the wall is permeable and the permeation velocity, U_P(=U_y in this case), is known, then

$$\rho U_P = \sum_i (f_i\mathbf{c}_i)_y = f_2^p + f_5^p + f_6^p \tag{31}$$

$$0 = \sum_{\mathbf{c}_i\cdot\mathbf{n}>0} (f_i^w\mathbf{c}_i)_x = f_5^p - f_6^p. \tag{32}$$

Additional constraint is needed to determine f_2^p, f_5^p, and f_6^p. Here the non-equilibrium bounce-back scheme in normal direction is applied [20]. Thus,

$$f_2^p = \frac{2}{3}\rho U_y, \qquad f_5^p = f_6^p = \frac{1}{6}\rho U_y. \tag{33}$$

The only unknown now is ρ, which can be determined by

$$\rho \equiv \sum_i f_i = f_0 + f_1 + f_3 + 2(f_4 + f_7 + f_8) + \rho U_y$$

$$\rho = \frac{f_0 + f_1 + f_3 + 2(f_4 + f_7 + f_8)}{1 - U_y}. \tag{34}$$

In summary,

$$f_2 = f_4 + \frac{2}{3}\rho U_y \tag{35}$$

$$f_5 = \sigma' f_7 + (1-\sigma')f_8 + \frac{\sigma'}{2}[\rho U_W - (f_1 - f_3)] + \frac{1}{6}\rho U_y \tag{36}$$

$$f_6 = \sigma' f_8 + (1-\sigma')f_7 \ -\frac{\sigma'}{2}[\rho U_W - (f_1 - f_3)] + \frac{1}{6}\rho U_y. \tag{37}$$

The implementation has some important features. The presence of U_W indicates that the new scheme deals with moving boundary conditions directly. This is indeed an important result. If the refereecne frame moves with the wall velocity like [22], when the populations of interior nodes propagate to the boundary nodes, one has to make transformations of f_i on the boundary nodes so that all values of f_i are counted on the same reference frame. Moreover, the representation of f_i^{eq} in the moving frame may not be the same as that in the stationary frame. The present scheme applies the same stationary frame to all nodes and no such transformation is necessary.

In addition, one should notice the presence of f_1 and f_3. In order to implement the slip and/or nonslip boundaries more correctly, f_1 and f_3 should be considered since they are involved in the calculation of the fluid velocity and then will affect the slip velocity in LBM. For nonslip boundaries ($\sigma' = 1$), it recovers the results by [20,21].

This scheme can also determine the unknown distributions of the corner nodes uniquely, no need to additionally assume the constant density at the corner nodes, as done in [20]. As an illustration, consider the lower-left corner of an impermeable, stationary boundaries, $U_W = U_P = 0$. The unknown distributions are f_1, f_2, f_5, f_6, and f_8. From the non-equilibrium bounce-back scheme in the normal directions, one can get

$$f_1 = f_3, \qquad f_2 = f_4. \tag{38}$$

If considering the lower boundary, the zero vertical velocity requires $f_5 + f_6 = f_7 + f_8$. On the other hand, if considering the left boundary, the zero horizontal velocity requires $f_5 + f_8 = f_6 + f_7$. These two constraints lead to

$$f_5 = f_7, \qquad f_6 = f_8. \tag{39}$$

Substituting into Eq. (37), one gets

$$f_6 = \sigma' f_6 + (1-\sigma')f_7. \tag{40}$$

Thus,

$$0 = (1-\sigma')(f_6 - f_7). \tag{41}$$

To solve f_6 and f_7 for arbitrary σ', it requires $f_6 = f_7$. It explains why Zou and He [20] could not determine the unknowns uniquely because for nonslip boundary conditions ($\sigma' = 1$), Eq. (41) becomes trivial and leaves f_6 and f_7 undetermined.

5. Numerical results

The Couette flows and planar Poiseuille flows are performed as benchmark tests for the present scheme.

5.1. Couette flows

Consider a steady Couette flow with the upper plate moving at constant speed U_W and the lower plate stationary. The distance between two plates is H. The simulation uses the nodes of $N_x \times N_y = 11 \times 11$ with periodic boundary conditions in the horizontal direction. The spacing between two plates is then $H = N_y - 1 = 10$. The velocity profile at steady-state should be linear. Suppose σ' of the upper plate is given. Without loss of the generality, the lower plate is assumed nonslip ($\sigma' = 1$). Thus, the slip velocity, $U(y = H) - U_W$, can be determined by

$$\frac{\partial U}{\partial y} = \frac{U(y=H)}{H} = \text{const} \tag{42}$$

$$U(y = H) - U_W = \frac{1-\sigma'}{\sigma'}\lambda\frac{\partial U}{\partial n}\bigg|_{y=H}. \tag{43}$$

Fig. 1 shows the normalized steady-state velocity profiles (U/U_W) under different values of σ'. The linear velocity profiles are verified. For $\sigma' = 1$, the simulation captures the nonslip boundary condition. In addition, one can see that the slip velocity is not linear with σ'. For $\sigma' \geqslant 0.5$, the slip velocity is less 5%.

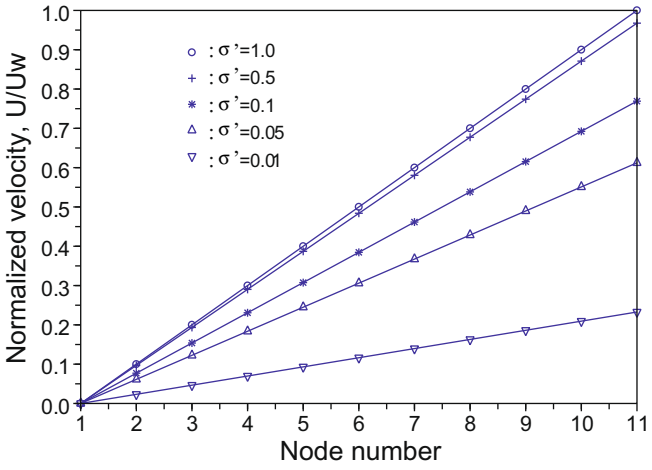

Fig. 1. Steady-state normalized velocity profiles for different σ' with $\tau = 1$. The straight lines are the fitting lines.

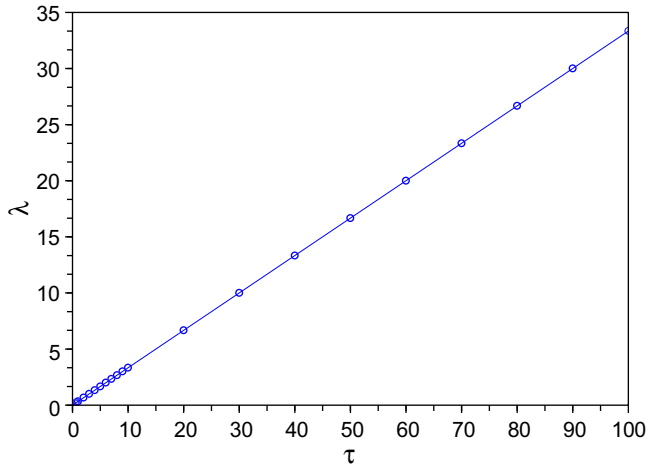

Fig. 3. Dependence of the mean free path (λ) on the relaxation time (τ) for $\sigma' = 1/2$. The slope of the fitting straight line is 1/3.

Recall that the Knudsen number is defined as $Kn \equiv \lambda/H$, therefore,

$$Kn = \frac{\lambda}{H} = \frac{\sigma'}{1-\sigma'}\left(\frac{U_W}{U(y=H)} - 1\right). \tag{44}$$

Note that the mean free path depends on the collision frequency. Therefore, Kn would depend on τ, but it should be independent of σ'. Fig. 2 presents the calculated Kn at different σ' under $\tau = 1$. The horizontal line indicates that Kn is independent of σ', as expected. The value of Kn is equal to 1/30. This means that $\lambda = Kn\ H = 1/3$.

The simulation results suggest that the Couette flow can be used to determine the mean free path in LBM for different relaxation time τ. Fig. 3 presents λ as a function of the relaxation time τ at fixed $\sigma' = 1/2$. The relation is linear and the slope is 1/3.

$$\lambda = \frac{1}{3}\tau, \qquad Kn = \frac{1}{3}\frac{\tau}{H}. \tag{45}$$

From the macroscopic point of view, λ is related to $\nu = \frac{1}{3}(\tau - 1/2)$. The numerical result shows that no 1/2 shift is necessary.

5.2. Planar Poiseuille flows

Consider a planar Poiseuille flow within two horizontal stationary plates with same σ'. The spacing between the plates is H. The simulation uses the nodes of $N_x \times N_y = 101 \times 11$. Pressure boundary conditions are imposed at the inlet and the exit. The steady-state velocity profiles for the flow are parabolic for Poiseuille flows. Applying Eq. (12) to both plates, one can get the normalized velocity profiles as

$$\frac{U(y)}{U_0} = 4(Y - Y^2) + \overline{U}_s \tag{46}$$

$$\overline{U}_s = \frac{U(y=0)}{U_0} = 4\frac{1-\sigma'}{\sigma'}Kn \tag{47}$$

where $Y = y/H$, U_0 is the maximum velocity under nonslip boundary conditions, and $\overline{U}_s$ is the normalized slip velocity.

Fig. 4 shows the normalized velocity profiles at the exit for $\tau = 1$. The profiles fit well the parabolic shapes. It is obvious that the slip velocity is larger for smaller σ'. Fig. 5 presents the normalized slip velocity as a function of σ'. One can see that Eq. (47) can well fit the simulation results if the Knudsen number is calculated by Eq. (45). This indicates that the present scheme can well implement a first-order slip model.

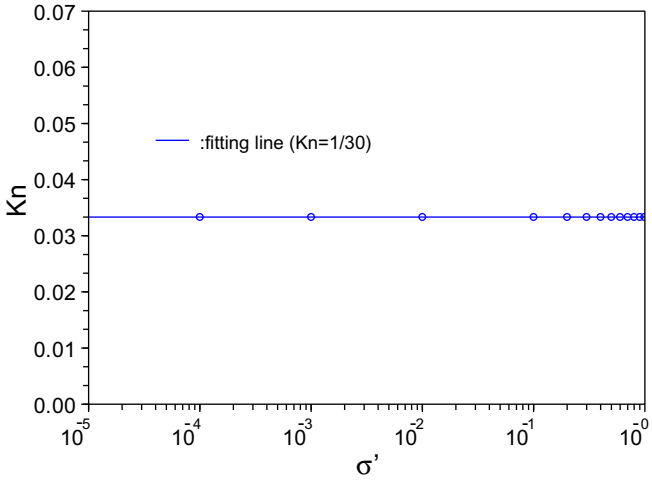

Fig. 2. Knudsen number as a function of σ' for $\tau = 1$. The results indicate that Kn is independent of σ'.

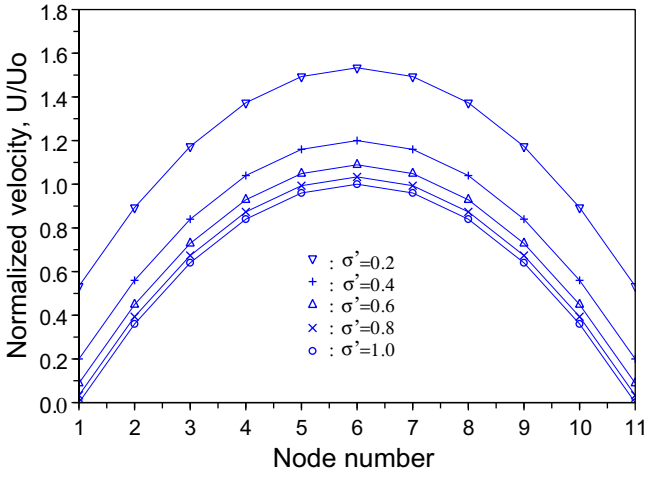

Fig. 4. The steady-state normalized velocity of a Poiseuille flow ($\tau = 1$) at the exit for various σ'.

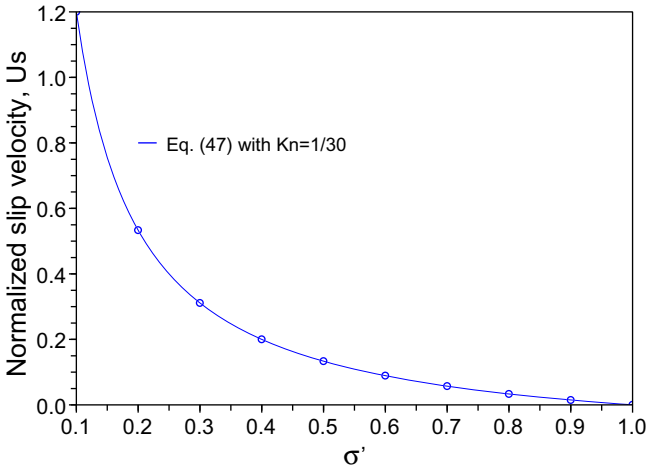

Fig. 5. The normalized slip velocity as a function of σ' at the exit. The Knudsen number is calculated based on Eq. (45).

6. Conclusion

A unified implementation for nonslip and slip boundary conditions in LBM were proposed and verified. With a given modified TMAC σ', the change of the tangential momentum of the fluid caused by the interactions can be calculated. Therefore, one can impose the corresponding boundary conditions in LBM. Couette flows and planar Poiseuille flows were studied under different slip conditions. When $\sigma' = 1$, the simulations produce the nonslip results. For $\sigma' < 1$, the numerical results demonstrate that the present scheme imposes the first-order slip model. Contrast to the works placing the physical boundaries between nodes, the present study made fair comparisons between numerical and theoretical work directly without any extrapolations. The fact of using the same stationary frame for all nodes makes the calculations simpler compared with the scheme applying the moving frame on the boundary nodes.

Acknowledgement

The authors thank the financial support of the National Science Council of Taiwan, Republic of China under Contract No. NSC96-2628-E-002-197-MY3.

References

[1] He XY, Zou QS, Luo LS, Dembo M. Analytic solutions of simple flows and analysis of nonslip boundary conditions for the lattice Boltzmann BGK model. J Statist Phys 1997;87:115–36.
[2] Ziegler DP. Boundary-conditions for lattice Boltzmann simulations. J Statist Phys 1993;71:1171–7.
[3] Aidun CK, Lu YN. Lattice Boltzmann simulation of solid particles suspended in fluid. J Statist Phys 1995;81:49–61.
[4] Inamuro T, Yoshino M, Ogino F. Non-slip boundary-condition for lattice Boltzmann simulations. Phys Fluids 1995;7:2928–30.
[5] Inamuro T, Yoshino M, Ogino F. A non-slip boundary condition for lattice Boltzmann simulations. Phys Fluids 1996;8:1124 (vol 7, pg 2928, 1995).
[6] Filippova O, Hanel D. Lattice-Boltzmann simulation of gas-particle flow in filters. Comput Fluids 1997;26:697–712.
[7] Shan XW. Simulation of Rayleigh-Benard convection using a lattice Boltzmann method. Phys Rev E 1997;55:2780–8.
[8] Rohde M, Kandhai D, Derksen JJ, Van den Akker HEA. Improved bounce-back methods for no-slip walls in lattice-Boltzmann schemes: Theory and simulations. Phys Rev E 2003;67:066703.
[9] Nie XB, Doolen GD, Chen SY. Lattice-Boltzmann simulations of fluid flows in MEMS. J Statist Phys 2002;107:279–289a.
[10] Succi S. Mesoscopic modeling of slip motion at fluid–solid interfaces with heterogeneous catalysis. Phys Rev Lett 2002;89:064502.
[11] Sbragaglia M, Succi S. Analytical calculation of slip flow in lattice Boltzmann models with kinetic boundary conditions. Phys Fluids 2005;17:093602.
[12] Sofonea V, Sekerka RF. Boundary conditions for the upwind finite difference lattice Boltzmann model: evidence of slip velocity in micro-channel flow. J Comput Phys 2005;207:639–59.
[13] Zhang YH, Gu XJ, Barber RW, Emerson DR. Capturing Knudsen layer phenomena using a lattice Boltzmann model. Phys Rev E 2006;74:046704.
[14] Guo ZL, Zhao TS, Shi Y. Physical symmetry, spatial accuracy, and relaxation time of the lattice Boltzmann equation for microgas flows. J Appl Phys 2006;99:074903.
[15] Benzi R, Biferale L, Sbragaglia M, Succi S, Toschi F. Mesoscopic two-phase model for describing apparent slip in micro-channel flows. Europhys Lett 2006;74:651–7.
[16] Benzi R, Biferale L, Sbragaglia M, Succi S, Toschi F. Mesoscopic modelling of heterogeneous boundary conditions for microchannel flows. J Fluid Mech 2006;548:257–80.
[17] Kim HM, Kim D, Kim WT, Chung PS, Jhon MS. Langmuir slip model for air bearing simulation using the lattice Boltzmann method. IEEE Trans Magn 2007;43:2244–6.
[18] Arkilic EB, Breuer KS, Schmidt MA. Mass flow and tangential momentum accommodation in silicon micromachined channels. J Fluid Mech 2001;437:29–43.
[19] Maxwell J. On stresses in rarified gases arising from inequalities of temperature. Phil Trans R Soc Lond 1879;170:231–56.
[20] Zou QS, He XY. On pressure and velocity boundary conditions for the lattice Boltzmann BGK model. Phys Fluids 1997;9:1591–8.
[21] Lamura A, Gonnella G. Lattice Boltzmann simulations of segregating binary fluid mixtures in shear flow. Phys A 2001;294:295–312.
[22] Ansumali S, Karlin IV. Kinetic boundary conditions in the lattice Boltzmann method. Phys Rev E 2002;66:026311.